NASA TECHNICAL MEMORANDUM

NASA TM X-62,179

NASA TM X-62,179

A THEORETICAL AND EXPERIMENTAL INVESTIGATION OF FLAP–LAG STABILITY OF HINGELESS HELICOPTER ROTOR BLADES

Robert A. Ormiston and William G. Bousman

Ames Research Center
and
U.S Army Air Mobility R&D Laboratory
Moffett Field, Calif 94035

August 1972

SYMBOLS

a	= two-dimensional lift curve slope
A, C	= induced flow parameters, Eq. (11)
b	= number of blades
c	= blade chord, m
c_{d_o}	= profile drag coefficient
D	= drag parameter, Eq. (13)
I	= blade inertia, $\frac{1}{3}$ mR^3, kg-m^2
K_{β_H}, K_{ζ_H}	= flap and lead-lag spring rates at hub, n-m /rad, Fig. 2
K_{β_B}, K_{ζ_B}	= flap and lead-lag spring rates at blade root, n-m /rad, Fig. 2
K_β, K_ζ	= total flap and lead-lag hinge spring rates at $\theta = 0$, n-m /rad, Eq. (8)
m	= blade mass distribution, kg/m
p, P, q	= rotating flap and lead-lag frequency parameters, Eqs. (3), (13), (4).
R	= blade radius, m; also, variable elastic coupling parameter, Eq. (10)
R_w	= elastic coupling parameter, Eq. (6)
s	= Laplace transform variable, sec^{-1}
W	= lead-lag frequency parameter, Eq. (13)
x, y, z	= rotating coordinates
z	= elastic coupling term, Eq. (5)
β	= flapping angular displacement of blade measured from plane of rotation, rad
γ	= Lock number, $\rho acR^4/I$
Δ	= elastic coupling parameter, Eq. (6)
ζ	= lead-lag or inplane angular displacement of blade, rad
η_m	= structural damping parameter
θ	= blade pitch angle, rad
θ_{min}	= minimum θ for neutral stability for given p

θ^* = absolute minimum θ for neutral stability

θ_ζ = kinematic pitch-lag coupling parameter

ρ = air density, kg/m^3

σ = rotor solidity, $bc/\pi R$

σ_ζ = real part of lead-lag mode eigenvalue, sec^{-1}

Ω = coordinate system angular velocity, rad/sec

ω = imaginary part of eigenvalue, rad/sec

ω_1, ω_2 = nonrotating flap and lead-lag frequencies, Eq. (19), rad/sec

$\omega_\beta, \omega_\zeta$ = flap and lead-lag non-rotating frequencies at $\theta = 0°$, Eq. (7), rad/sec

$( )_o, \Delta( )$ = steady state and perturbation variables

$\bar{( )}$ = nondimensionalized by R for lengths, $R\Omega$ for velocities Ω for frequencies

A THEORETICAL AND EXPERIMENTAL INVESTIGATION OF FLAP-LAG STABILITY OF HINGELESS HELICOPTER ROTOR BLADES

Robert A. Ormiston and William G. Bousman
Ames Directorate
U. S. Army Air Mobility Research & Development Laboratory
Moffett Field, CA 94035

SUMMARY

The stability of hingeless rotor blade oscillations in hover is examined theoretically using a simplified centrally-hinged, spring-restrained, rigid blade to approximate the deflections of actual elastic blades. The aerodynamic and inertial coupling between the flap and lead-lag degrees of freedom is primarily responsible for instability, however elastic coupling and kinematic pitch-lag coupling both exert a powerful influence on hingeless rotor blade stability. Experimental results obtained from a two-bladed 1.81m diameter model rotor designed for minimum elastic coupling have confirmed the results of linear theory. For this model configuration rotor blade stall at high pitch angles was found to counteract the destabilizing flap-lag coupling and increase the damping of lead-lag oscillations. It was possible to account for this effect with the theory by using drag data for stalled airfoils.

INTRODUCTION

The hingeless rotor has become an attractive concept for conventional and compound helicopters in recent years. The primary reasons are that increased control power and angular damping of the hingeless rotor substantially enhance flying qualities and maneuverability, and the simpler hub design

reduces maintenance and improves reliability. Experience with hingeless rotors, however, has revealed a number of unexpected and potentially catastrophic rotor blade instabilities. These instabilities were not previously encountered with conventional articulated rotor helicopters and are partly attributable to the lack of adequate basic research on the dynamics of hingeless rotors.

For clarity, these instabilities may be loosely divided into three classes. The first and most fundamental of these is characterized by the exclusion of translation or angular rotation of the fuselage, in other words, the rotor hub is fixed. The individual blades are thus uncoupled and the relevant degrees of freedom are the flap, lead-lag, and torsional deflections measured with respect to a coordinate system rotating with the rotor shaft. The second class includes the fuselage degrees of freedom and is characterized by coupled rotor-fuselage dynamics. The motions of all the rotor blades are coupled to one another in addition to fuselage motion because of the hub freedom. The the third class covers problems which incorporate feedback control systems. Although usually applied to the fuselage motion dynamics, these control systems may induce serious instabilities of the rotor blade degrees of freedom, particularly the weakly damped lead-lag motion. Although not so important for articulated rotors, this classification has a unique significance for hingeless rotors. This is directly attributable to the strong elastic coupling between the rotor and fuselage degrees of freedom in addition to coupling between the flap, lead-lag, and torsion degrees of freedom of each individual blade. Ultimately, therefore, these couplings are a potential source of various instabilities for hingeless rotor helicopters. Equally possible, however, they offer considerable potential for improving rotor stability once the dynamics

of hingeless rotors are better understood.

Within this classification, the individual blade degrees of freedom are the heart of the fully coupled rotor/fuselage/control system dynamics problem. Therefore, a complete understanding of hingeless rotor helicopter dynamics can only be obtained by first thoroughly investigating the stability characteristics of the fundamental blade degrees of freedom. A special subclass of this problem known as flap-lag stability is treated in the present study. In this case, the torsional degree of freedom is excluded to afford a clearer understanding of the aerodynamic, inertial, and elastic coupling between the flap and lead-lag degrees of freedom. Although this problem has been examined in previous research, not all of the important rotor parameters have been identified or systematically investigated.

In the absence of available experimental data a model rotor was designed and tested to complement thetheoretical analysis. As a result of these investigations several practical approaches can now be suggested for improving the inherent stability of hingeless rotor blades.

THEORETICAL ANALYSIS

Equation of Motion

The basic flap and lead-lag deflections of a hingeless rotor blade are measured with respect to an x, y, z, coordinate system positioned in the undeformed blade and rotating with angular velocity Ω, Fig. 1. The axis of rotation is fixed in space and the blades are considered rigid in torsion. In order to eliminate periodic coefficients in the aerodynamic and elastic terms of the equations of motion, the problem is restricted to hover and excludes

cyclic pitch inputs. Although the motion of an actual elastically deflected rotor blade shown in Fig. 1 must be described by partial differential equations, considerable simplification can be obtained by replacing the elastic blade with an appropriately hinged rigid blade shown in Fig. 2 where spring elements are used to simulate the elastic properties of the actual rotor blade. The problem is then reduced to one involving only ordinary differential equations* which are both easier to solve and considerably easier to interpret in physical terms.

An important feature of hingeless rotor blades is that when the collective pitch angle changes, the elastic principle axes of the portion of the blade outboard of the pitch bearing also rotate, thus altering the relative stiffnesses in the flapping and lead-lag directions. Furthermore, this rotation couples these degrees of freedom elastically, that is, flap deflections produce lead-lag bending moments and vice-versa. The degree of this elastic coupling is strongly dependent on the radial position of the pitch change bearing, Fig. 1, or in other words the relative blade flexibility occurring inboard and outboard of the pitch bearing.

The importance of this coupling requires that the flap and lead-lag hinge springs of the rigid blade representation be divided into two distinct orthogonal systems -- one located inboard and one outboard of the pitch bearing, as shown in Fig. 2. The degree of elastic coupling is determined by the relative flexibilities of these two spring systems. Although the pitch bearing location is an important design parameter for hingeless rotor helicopters the associated elastic coupling effects have not been previously recognized as a significant factor in flap-lag stability.

*The exact partial differential equations for the flap-lag problem are presented and compared with the present approximate equations in Ref. 1. The results indicate good accuracy for the approximate equations.

The differential equations of motion for the flap and lead-lag angular deflections (β,ζ) for the rigid blade representation of the hingeless rotor are obtained by summing the flap and lead-lag moments due to aerodynamic, inertial, and elastic forces. A complete derivation is given in Ref. 1. Since the equations are nonlinear, it is advantageous to consider the stability of small deflections from the equilibrium condition. The equations for the flap and lead-lag perturbation deflections ($\Delta\beta$, $\Delta\zeta$) are thereby linearized about the equilibrium delfections (β_o, ζ_o) .

The equilibrium equations are given by

$$\begin{bmatrix} p^2 & z^2 \\ z^2 & q^2 \end{bmatrix} \begin{Bmatrix} \beta_o \\ \zeta_o \end{Bmatrix} = \gamma/8 \begin{Bmatrix} \theta - A \\ -\left(\frac{c_{d_o}}{a} + A\theta - C\right) \end{Bmatrix} \qquad (1)$$

and the Laplace transformed perturbation equations are

$$\begin{bmatrix} s^2 + \frac{\gamma}{8} s + p^2 & -s\left[\frac{\gamma}{8}(2\theta-A)-2\beta_o\right] + z^2 \\ -s\left[2\beta_o - \frac{\gamma}{8}(\theta-2A)\right] + z^2 & s^2 + s\frac{\gamma}{8}\left(2\frac{c_{d_o}}{a} + A\theta + \frac{16\eta_m\bar{\omega}_\zeta}{\gamma}\right) + q^2 \end{bmatrix} \begin{Bmatrix} \Delta\beta \\ \Delta\zeta \end{Bmatrix}$$

$$= \Delta\theta \left[\frac{\gamma}{8} \begin{Bmatrix} 1 \\ -A \end{Bmatrix} - R\frac{(\bar{\omega}_\zeta^2 - \bar{\omega}_\beta^2)}{\Delta} \left\{ R_w \begin{bmatrix} \left[\beta_o - \frac{\gamma}{8}(\theta-A)\right] \\ \frac{\gamma}{8}\left(\frac{c_{d_o}}{a} + A\theta - C\right) \end{bmatrix} + \beta_o \begin{bmatrix} \sin 2\theta \\ \cos 2\theta \end{bmatrix} + \zeta_o \begin{bmatrix} \cos 2\theta \\ -\sin 2\theta \end{bmatrix} \right\} \right] \qquad (2)$$

where

$$p^2 = 1 + \frac{1}{\Delta}\left[\bar{\omega}_\beta^2 + R(\bar{\omega}_\zeta^2 - \bar{\omega}_\beta^2)\sin^2\theta\right] \tag{3}$$

$$q^2 = \frac{1}{\Delta}\left[\bar{\omega}_\zeta^2 - R(\bar{\omega}_\zeta^2 - \bar{\omega}_\beta^2)\sin^2\theta\right] \tag{4}$$

$$z^2 = \frac{R}{2\Delta}(\bar{\omega}_\zeta^2 - \bar{\omega}_\beta^2)\sin 2\theta \tag{5}$$

$$\Delta = 1 + R(1-R)\frac{[\bar{\omega}_\zeta^2 - \bar{\omega}_\beta^2]^2}{\bar{\omega}_\zeta^2\bar{\omega}_\beta^2}\sin^2\theta \quad , \quad R_w = (1-R)\frac{[\bar{\omega}_\zeta^2 - \bar{\omega}_\beta^2]^2}{\bar{\omega}_\zeta^2\bar{\omega}_\beta^2}\sin 2\theta \tag{6}$$

$$\bar{\omega}_\beta^2 = K_\beta/I\Omega^2 \quad , \quad \bar{\omega}_\zeta^2 = K_\zeta/I\Omega^2 \tag{7}$$

$$K_\beta = \frac{K_{\beta_B}K_{\beta_H}}{K_{\beta_B} + K_{\beta_H}} \quad , \quad K_\zeta = \frac{K_{\zeta_B}K_{\zeta_H}}{K_{\zeta_B} + K_{\zeta_H}} \tag{8}$$

$$R_\beta = K_\beta/K_{\beta_B} \quad , \quad R_\zeta = K_\zeta/K_{\zeta_B} \tag{9}$$

$$R = \frac{\bar{\omega}_\zeta^2 R_\beta - \bar{\omega}_\beta^2 R_\zeta}{\bar{\omega}_\zeta^2 - \bar{\omega}_\beta^2} \tag{10}$$

The terms associated with aerodynamic forces are the Lock number γ, profile drag coefficient c_{d_o}, lift curve slope a, and the induced inflow parameters A and C which are approximated using momentum theory, Ref. 2.

$$A = \frac{a\sigma}{12}\left[\sqrt{1 + \frac{24\theta}{a\sigma}} - 1\right] \quad , \quad C = A^2 \tag{11}$$

The collective pitch angle is given by θ. The Coriolis and centrifugal inertial forces arise from the equilibrium flap deflection or coning, β_o.

The remaining terms involve elastic forces which are unique to the hingeless rotor. The non-rotating flap and lead-lag frequencies $\bar{\omega}_\beta$ and $\bar{\omega}_\zeta$ broadly define various classes of hingeless rotor blade configurations. For instance soft inplane rotors are characterized by $\bar{\omega}_\zeta < 1.0$ and stiff inplane rotors by $\bar{\omega}_\zeta > 1.0$. The parameter R is used to define the degree of elastic coupling. For R = 0.0, the blade flexibility is located inboard of the pitch bearing and no elastic coupling is introduced as pitch angle is increased from zero. The converse is true for R = 1.0 while intermediate values of R define varying degrees of elastic coupling.

The stability of flap and lead-lag motions defined by these equations will be examined for three distinct cases: 1) basic flap-lag coupling (R = 0.0), 2) the effects of variable elastic coupling ($R \neq 0.0$), and 3) the influence of kinematic pitch-lag coupling.

Basic Flap-Lag Stability

The homogeneous portion of Eq. (2) governs the basic flap-lag stability of hingeless rotors. For R = 0.0, coupling between the flap and lead-lag degrees of freedom is due only to aerodynamic and inertial forces, the single underlined terms in Eq. (2). The damping in the lead lag equation is inherently very small since it consists of only profile drag damping, induced inflow damping, and structural damping. Under certain conditions, the product of the basic aerodynamic and inertial flap-lag coupling terms is destabilizing and may provoke an instability of the weakly damped lead-lag mode. This is shown in Fig. 3 which is a locus of roots of the flap-lag characteristic equation plotted in the complex plane. The loci trace the roots of the flap

and lead-lag modes as collective pitch is increased from 0.0 to 0.5 rad for several configurations having various lead-lag frequencies. When $\bar{\omega}_\zeta$ is close to the rotating flap frequency ($p = \sqrt{4/3} = 1.1547$), the lead-lag mode becomes unstable. In Fig. 3 as well as the next four figures, the rotor parameters are as follows: $\gamma = 5.0$, $\sigma = 0.05$, $c_{d_o} = 0.01$, $\eta_m = 0.0$.

Although the unstable configurations do not represent typical designs (other constraints preclude the $\bar{\omega}_\zeta \simeq p$ configuration) these results do afford insight into the physical mechanisms which govern the stability of hingeless rotor blades. For instance, Routh's criterion for the neutral stability condition can be used to derive a formula for the smallest collective pitch angle at which the rotor blade will become unstable. Thus we have

$$(\theta - A)^2 = \frac{P^2}{2(P-1)(2-P)} \left\{ D + \frac{(D+A\theta)(P-W)^2}{(\gamma/8)^2[W+P(D+A\theta)](1+D+A\theta)} \right\} \tag{12}$$

where

$$D = 2\left[\frac{c_{d_o}}{a} + \frac{8\eta_m \bar{\omega}_\zeta}{\gamma}\right] \quad ; \quad P = p^2 \quad ; \quad W = \bar{\omega}_\zeta^2 \tag{13}$$

Since $D \geq 0$ and $A\theta \geq 0$, it follows that a necessary (but not sufficient) condition for instability is that $1 < p^2 < 2$. This indicates that simple, centrally-hinged articulated rotors cannot be unstable since $p = 1$. In addition, for a given flapping frequency, p, the minimum collective pitch for neutral stability, θ_{min}, occurs when $\bar{\omega}_\zeta = p$.

$$(\theta_{min} - A)^2 = \frac{P^2 D}{2(P-1)(2-P)} \tag{14}$$

For $p = \sqrt{4/3}$ an absolute minimum occurs in the collective pitch for neutral

stability. This value, referred to as θ^* is

$$(\theta^*-A)^2 = 4D = 8\left[\frac{c_{d_o}}{a} + \frac{16\sqrt{3}}{3}\frac{\eta_m}{\gamma}\right] \tag{15}$$

These simple and concise relations clearly show the dependence of flap-lag stability on the basic system parameters and design variables.

Both profile drag and structural damping are stabilizing, as is the induced inflow represented by the parameter A. Since induced inflow increases with rotor solidity, σ, increased blade chord or number of blades is stabilizing. When $p \neq \bar{\omega}_\zeta$ the stability depends on the combination of p and $\bar{\omega}_\zeta$, together with the Lock number. This dependency is shown in Fig. 4, which maps the neutral stability boundaries as a function of flap and lead-lag frequencies. For a particular collective pitch the region of instability lies within the respective contour. These results illustrate the occurrence of θ_{min} for a given value of p when $\bar{\omega}_\zeta = p$, and θ^* when $p = \sqrt{4/3}$ as indicated by Eqs. (14) and (15).

Effect of Variable Elastic Coupling

The elastic flap-lag coupling terms are doubly underlined in Eq. (2). They are roughly proportional to the collective pitch angle, the elastic coupling parameter R, and the difference between the flap and lead-lag nonrotating frequencies $(\bar{\omega}_\zeta^2 - \bar{\omega}_\beta^2)$. The importance of these terms for hingeless rotor blades is immediately apparent by comparing the locus of roots with elastic coupling in Fig. 5 with the previous case, Fig. 3. Only three lead-lag frequencies are shown, which typify practical soft-inplane $\bar{\omega}_\zeta = .7$ and stiff-inplane $\bar{\omega}_\zeta = 1.4$ rotor blade configurations. The third case, $\bar{\omega}_\zeta = 1.1$, is included for comparison. The

stiff inplane rotor blade is highly unstable for small values of R, while the lead-lag damping of the soft inplane rotor blade is increased. Values of R near 1.0 are highly stabilizing in both cases, but more so for the stiff inplane configuration. Stability boundaries as a function of lead-lag frequency and elastic coupling are shown in Fig. 6. This plot illustrates that the minimum pitch angle for instability is determined by a specific relationship between the lead-lag frequency and R.

Routh's criterion may again be used to investigate this case. For small pitch angles ($\theta^2 << 1$) the pitch angle for neutral stability is given by

$$(\theta-A)^2 = \frac{p^2}{2(P-1)(2-P)}\left\{ D + \frac{\left[D - \frac{(\theta-A)^2}{4}\right](W-P)^2 + \left[\frac{(\theta+A)(W-P)}{2} - R\theta(W-P+1)\right]^2}{\eta^2 W}\right\} \quad (16)$$

For simplicity consider the case $R_\beta = R_\zeta$. Since $0 \leq R \leq 1$, elastic coupling can only be destabilizing when $W > P$ or $W < P - 1$. This explains why only stiff inplane rotor blades become unstable in Figs. 5 and 6. When $p = \sqrt{4/3}$, the value of R corresponding to the least stable value of lead-lag frequency may be obtained from the following relation.

$$R = \frac{\theta^*+A}{2\theta^*} \frac{(\bar{\omega}_\zeta^2 - 4/3)}{(\bar{\omega}_\zeta^2 - 1/3)} \quad (17)$$

It is of interest that the pitch angle for this condition is precisely that given by Eq. (16) for basic flap-lag instability, i.e., θ^*, which explains why the minimum pitch angle for instability in Fig. 6 was independent of R and $\bar{\omega}_\zeta$.

The practical importance of elastic coupling is that while small values of R are potentially dangerous for stiff inplane rotor blades, large values of R provide a means of greatly increasing the inherently weak lead-lag damping of both soft and stiff inplane rotor blades. In the present state of the art of hingeless rotor design, no sound rationale exists regarding the influence of pitch bearing location and elastic coupling on rotor blade stability characteristics. Therefore, the present analysis could provide a basis for a rational approach toward improving the stability of hingeless rotors.

Pitch-Lag Coupling

Coupling between the blade pitch angle and the lead-lag deflection can be caused by either control system kinematics or coupled bending-torsion of the rotor blade. The former effect is a well known cause of articulated rotor instability. However, both factors are significant for hingeless rotors and have not been adequately studied. The present perturbation flap-lag equations including the nonhomogeneous terms may be used to investigate this subject. The necessary equation for pitch-lag coupling is given by $\Delta\theta = \theta_\zeta \Delta\zeta$ where θ_ζ is the magnitude of the coupling. In particular the combined effects of elastic coupling and pitch-lag coupling will be examined. The results are given in the form of stability boundaries for a soft and a stiff inplane configuration in Fig. 7. For the soft inplane case, the result is qualitatively similar to an articulated rotor, positive θ_ζ is destabilizing, and the effect of variable elastic coupling is found to be slight. The stiff inplane configuration, however, exhibits entirely different behavior. With no elastic coupling, negative θ_ζ produces instability. Elastic coupling, however, is strongly stabilizing for negative θ_ζ, but becomes progressively destabilizing as R increases and θ_ζ becomes positive. Therefore, potential instabilities can occur for various

combinations of pitch-lag coupling and elastic coupling. These results further emphasize the need for a rational approach to hingeless rotor design if instabilities arising from several combined coupling effects are to be avoided.

EXPERIMENT

The theory discussed above shows that flap-lag coupling can destabilize rotor blade lead-lag oscillations. As previous experimental work to support this conclusion is absent, an experimental model was designed and tested to determine if the reduction in damping predicted by the basic flap-lag theory did indeed occur for a real system. For the initial experiments reported below, it was decided to focus on the important but subtle aerodynamic and inertial coupling terms. To do this, a model configuration was chosen which minimized elastic coupling ($R \approx 0.0$), and hinge stiffnesses were chosen to assure penetration of the region of minimum stability shown in Fig. 4. Finally, the model configuration was patterned as closely as possible after the idealized representation of a hingeless rotor blade to insure maximum compatibility between the experimental and theoretical results.

Experimental Design

A sketch of the model hub is shown in Fig. 8. Flapping and lead-lag flexibility is contained in separate flexures, located as close to the hub centerline as possible. Elastic coupling of the flap and lead-lag motions is minimized by changing blade pitch angle outboard of the flexures and designing the blades themselves for maximum stiffness. This design closely approximates the theoretical representation of a centrally-hinged, spring-restrained, rigid blade. The only damping in the model hub is the structural damping in the flexures.

Torsional stiffness for each blade is provided by the two flap flexures which are displaced laterally from the blade centerline. The resulting torsional natural frequency is approximately twenty times as large as either the flapping or lead-lag natural frequencies, which, for practical purposes, eliminates the torsional degree of freedom. The flapping stiffness, K_β, and lead-lag stiffness, K_ζ, were selected so that the region of minimum stability could be penetrated. Fig. 4 shows this region as a function of nondimensional flapping and lead-lag frequencies, where

$$p = \sqrt{1 + \frac{K_\beta}{I\Omega^2}} \quad ; \quad \bar{\omega}_\zeta = \sqrt{\frac{K_\zeta}{I\Omega^2}} \tag{18}$$

By simply varying the rotor speed, Ω, it is possible to change p and $\bar{\omega}_\zeta$ simultaneously, and thereby traverse the region of minimum stability.

The rotor blades were constructed of balsa wood with an aluminum spar and covered with fiberglass. The major rotor parameters are given in Table 1.

Table 1

Lock number, γ	2.80
solidity, σ	0.0600
radius, R	0.905m
blade chord, c	0.0856m
airfoil section	NACA 0012
twist	-11.94 deg/m
Reynolds number	$1.0 - 2.5 \times 10^5$

The hub and blades were mounted on a rigid test stand as shown in Fig. 9, and driven by a pneumatic motor. To measure damping of the lead-lag motions, the rotor was excited with an electrodynamic shaker in the nonrotating system, and

the transient decay of the blade lead-lag oscillations was recorded after the shaker excitation was terminated.

Instrumentation

The blade root flexures were instrumented with strain gages to measure the flapping and lead-lag bending moments of both blades. In addition, the flap flexures on one blade were strain gaged to measure torsion moments. All gages were calibrated with applied moments so that angular deflection could be related directly to strain. The strain gage signals were removed from the rotating system with a forty channel set of slip rings (Fig. 9). The rotor speed was determined with an inductive pickup. Stand accelerations were monitored with an accelerometer mounted below the hub. All output signals were recorded on an oscillograph and magnetic tape (for subsequent data processing), and an oscilloscope was used to monitor significant parameters.

Nonrotating Tests

Nonrotating tests were run to determine rotor stiffness and inertia characteristics. With the rotor hub locked to prevent rotation, flapping and lead-lag motions were excited and the natural frequencies of the resulting blade oscillations were measured. In repeating these tests over a range of pitch angles from -2 degrees to 90 degrees, a small variation in the flapping and lead-lag natural frequencies was discovered. This variation occurred because the rotor blades are not perfectly rigid outboard of the pitch change bearing, and therefore a small amount of elastic coupling is present. The degree of this coupling was determined by finding the elastic coupling factor R which gave the best agreement between the experimental and theoretical nonrotating frequencies throughout the full pitch angle range. The theoretical frequencies are obtained from Eq (2) after eliminating the aerodynamic, centrifugal, and Coriolis terms from the homogeneous equations.

$$\omega_{1,2} = \sqrt{\frac{\omega_\beta^2 + \omega_\zeta^2}{2\Delta} \pm \sqrt{\frac{\left(\omega_\beta^2 + \omega_\zeta^2\right)^2}{4\Delta^2} - \frac{\omega_\beta^2 \omega_\zeta^2}{\Delta}}} \qquad (19)$$

The coupling factor giving best agreement was R = 0.11, and the associated theoretical and experimental frequencies are shown in Fig. 10.

The measured structural damping of the lead-lag oscillations was 0.11% critical, and was invariant for $0° \leq \theta \leq 18°$.

Rotating Tests

Rotating tests examined both steady state and transient operation. Steady values of blade coning and profile drag coefficient were measured to compare with theoretical predictions, and to estimate the limits of linearized theory. Fig. 11 shows the steady coning parameter as a function of collective pitch. The coning angle significantly departs from linear theory as the blade enters a stalled condition for collective pitch angles in the range of 12 to 14 degrees. Blade stall was observed experimentally in this region using wool tufts under stroboscopic illumination. This low stall angle is due to the low Reynolds number and is in good agreement with two-dimensional airfoil data, Ref. 3. As blade coning determines the extent of inertial flap-lag coupling, it is expected that the theory will overpredict the coupling effects at collective pitch angles above stall. The small increase in coning over the theoretical prediction for pitch angles below stall is due to ground effect which reduced the rotor downwash.

The mean profile drag coefficient calculated from the steady lead-lag deflection is shown in Fig. 12. The two-dimensional drag coefficient data of Ref. 3 is shown for comparison. The damping of the lead-lag motions is strongly dependent upon the mean profile drag coefficient, which is assumed to have a constant value in the linear theory. For higher collective pitch angles the linear theory will underestimate the amount of drag damping present.

The transient motion of the rotor blades during rotating tests was investigated by exciting the fixed hub in a direction parallel to the plane of rotation with an electrodynamic shaker at a frequency of $\Omega + \omega_\zeta$. In the rotating system, this excitation occurred at the lead-lag natural frequency. When the lead-lag oscillatory amplitude was sufficiently large, excitation was terminated and the damped transient motion of the oscillations was recorded on the oscillograph and magnetic tape. Measurements of lead-lag damping were made over a range of collective pitch angles and blade natural frequencies. Figure 13 shows the experimental nondimensional lead-lag damping as a function of nondimensional lead-lag natural frequency for a collective pitch angle of 11.95 degrees. The theory without flap-lag coupling simply shows the effects of structural, profile, and induced drag damping which increase the lead-lag damping as the pitch angle is increased. The effect of flap-lag coupling, however, is to significantly reduce the damping for nondimensional lead-lag natural frequencies near the flapping frequency. The experimental data confirm the predicted reduction due to aerodynamic and inertial flap-lag coupling. The effect of the small degree of elastic coupling is to shift the lead-lag frequency for minimum damping away from the frequency where $p = \bar{\omega}_\zeta$. The scatter in damping values at each lead-lag frequency is indicative of the difficulty in

measuring very small values of damping (less than 0.4% critical damping). Valid data could not be reliably obtained for $\bar{\omega}_\zeta < 1.2$ because flexibility of the rotor test stand at a resonant frequency introduced extraneous damping into the rotor blade oscillations.

Figure 14 compares the experimental and theoretical lead-lag damping as a function of collective pitch angle for $\bar{\omega}_\zeta = 1.278$. This is the approximate frequency for minimum stability. The theory without flap-lag coupling shows a steady increase in damping with collective pitch and does not correlate with the measured data. The complete linear flap-lag theory, however, correctly predicts the decrease in damping that occurs as collective pitch is increased to the stall angle. Beyond stall the linear flap-lag theory continues to predict a reduction in the lead-lag stability, however, if modified to include measured airfoil drag data, the theory then correctly shows the strongly stabilizing effect of the profile drag damping of the stalled rotor.

Concluding Remarks

Several general conclusions may be summarized from these results.

1. The theoretical analysis gives significant insight into the stability characteristics of hingeless rotor blades primarily because it is simple enough to easily comprehend while still retaining the essential rotor blade degrees of freedom. Instabilities were shown to be the result of aerodynamic and inertial coupling of the flap and lead-lag degrees of freedom.

2. With elastic coupling effects neglected, the least stable condition occurred when the lead-lag frequency was equal to the flap frequency and the flap frequency was $\sqrt{4/3}$. It was found that profile drag, structural damping, and aerodynamic

induced drag were stabilizing.

3. An experimental investigation confirmed that the theoretically destabilizing effects of aerodynamic and intertial flap-lag coupling actually occurred in a real system. Nonlinearities resulting from blade stall at high collective pitch angles increased lead-lag damping. The theory was also able to account for these nonlinearities.

4. The inclusion of flap-lag elastic coupling and kinematic pitch-lag coupling were found to have an important influence on the rotor blade stability. The elastic coupling is structurally inherent in all hingeless rotor blades but has not previously been recognized as an important factor in determining rotor blade flap-lag stability. The present theoretical analysis indicates that the degree of elastic coupling, depending on the lead-lag frequency, determines whether the rotor blade will be stable or unstable. The degree of elastic coupling is also shown to be dependent on several rotor blade design parameters, such as pitch bearing location and the blade flexibility distribution.

5. In practical terms the present results are encouraging because they permit a much needed understanding of hingeless rotor blade stability and should provide the basis for a rational approach to the design of hingeless helicopter rotors. For instance, configurations providing a high degree of elastic coupling can significantly improve lead-lag damping and a judicious choice of pitch-lag coupling can also be very beneficial.

The present work has stimulated the continuation of this research and several areas are currently under study. Experimental verification of the

high damping afforded by large elastic coupling is presently underway while theoretical efforts are aimed at studying the important effects of the torsional degree of freedom.

REFERENCES

1. Ormiston, R.A. and Hodges, D.H.; "Linear Flap-Lag Dynamics of Hingeless Rotor Blades in Hover, "Journal of the American Helicopter Society; Vol. 17, No. 2, April 1972.

2. Gessow, A. and Myers, G.D., Jr.; Aerodynamics of the Helicopter, Frederick Ungar Publishing Co., New York, 1967.

3. Jacobs, E.N. and Sherman, A.; "Airfoil Section Characteristics as Affected by Variations of the Reynolds Number," NACA Report No. 586, June 1936.

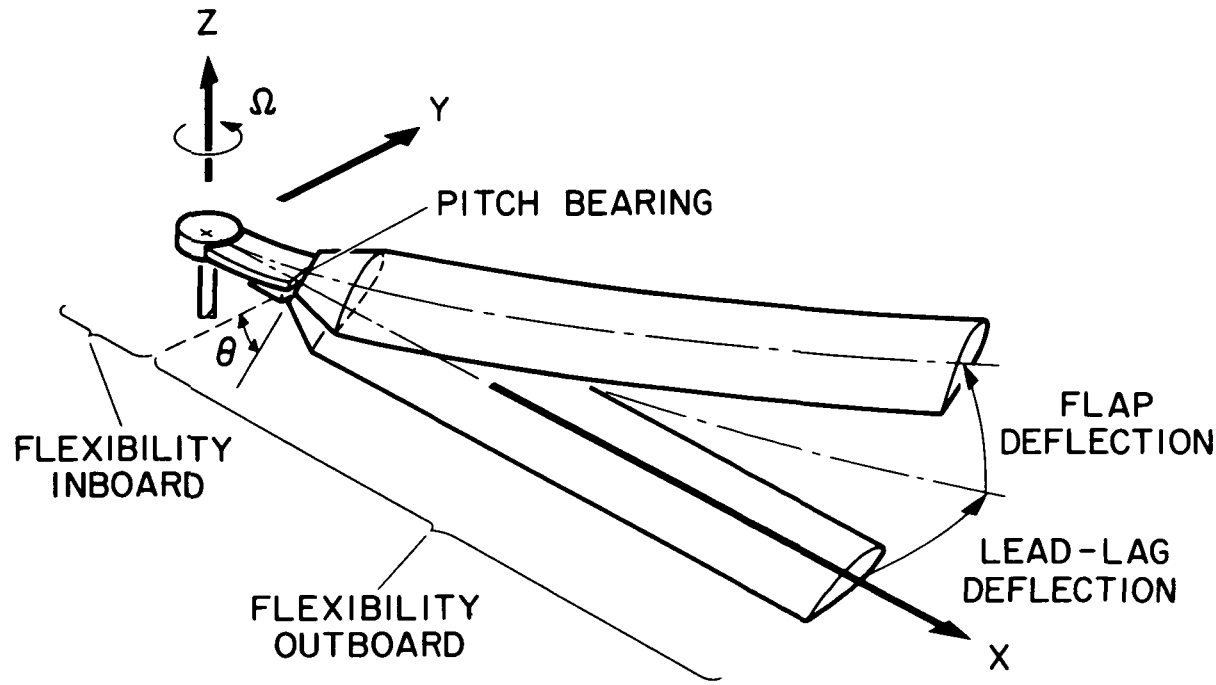

Figure 1. - Schematic representation of a hingeless rotor blade in rotating coordinate system, showing elastic bending deflections.

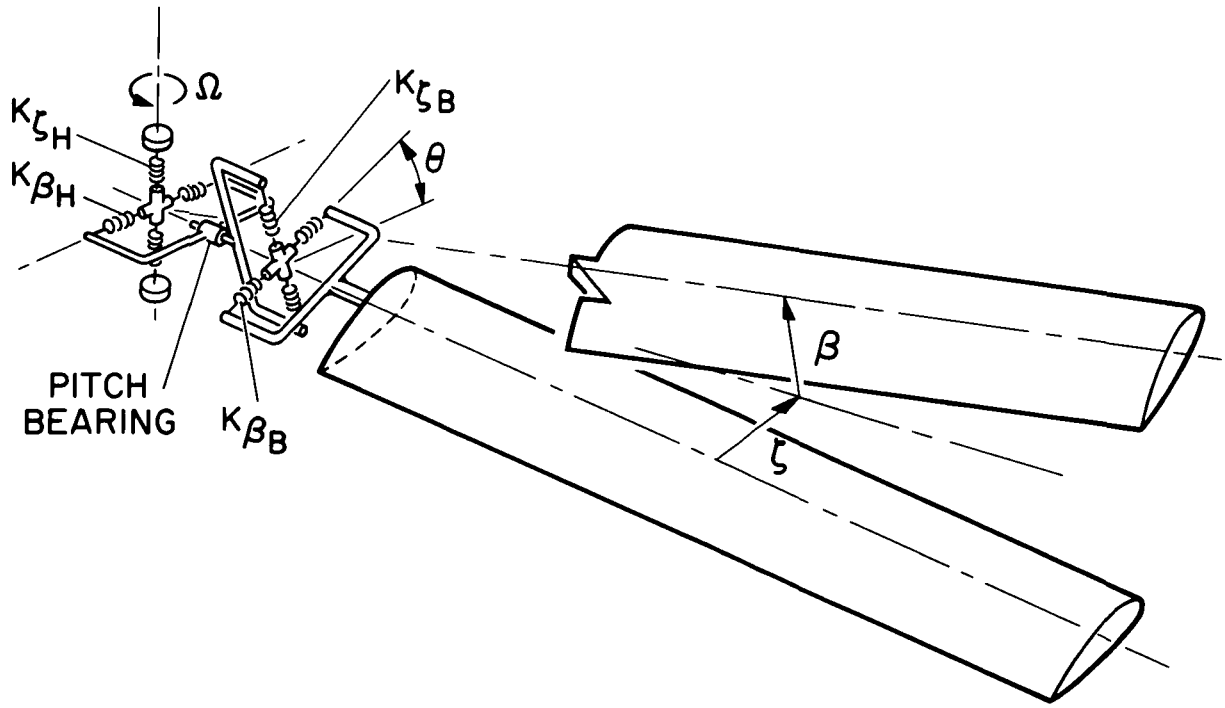

Figure 2. - Centrally-hinged, spring-restrained, rigid blade representation with spring stiffness arranged inboard and outboard of the pitch bearing.

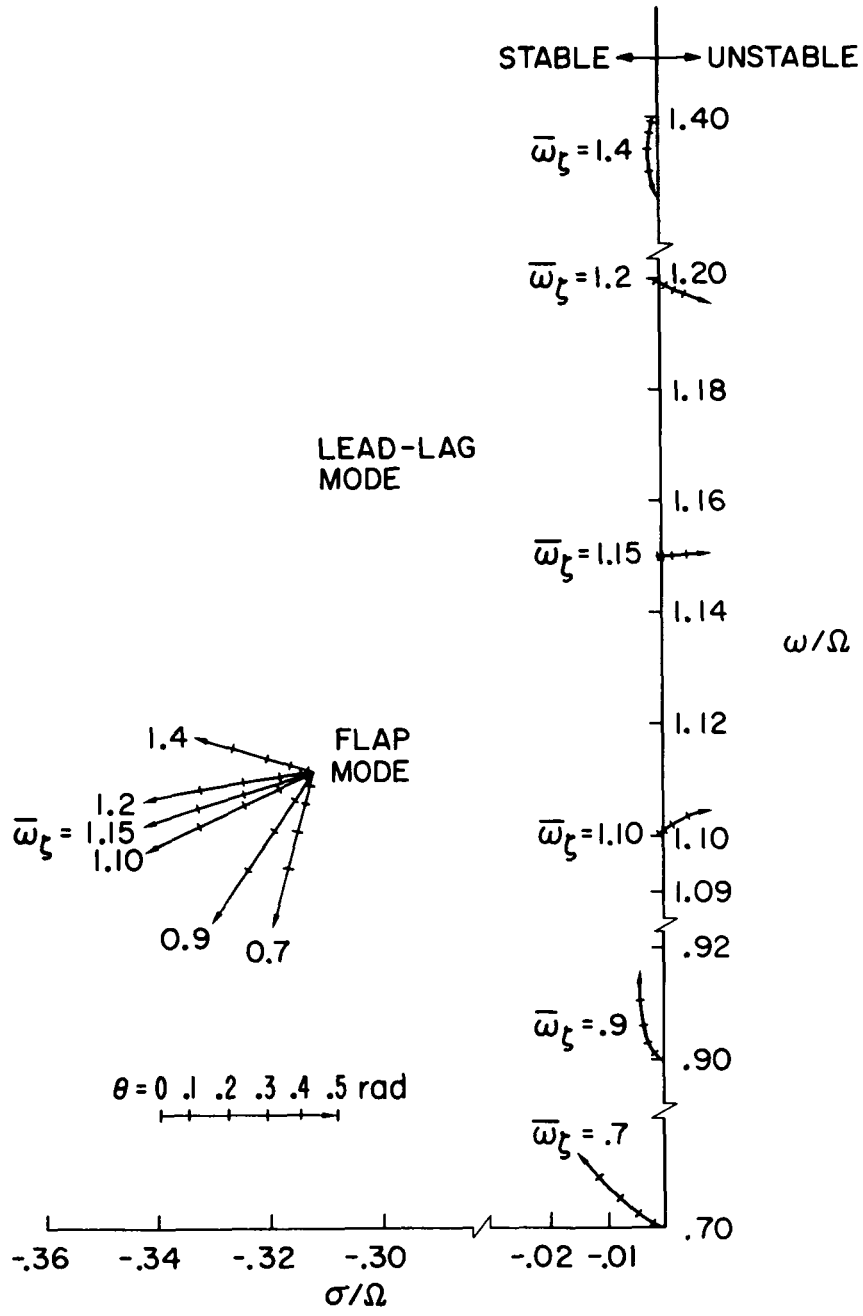

Figure 3. - Locus of roots with increasing pitch angle for basic flap-lag equations without elastic coupling, R = 0.0, p = $\sqrt{4/3}$

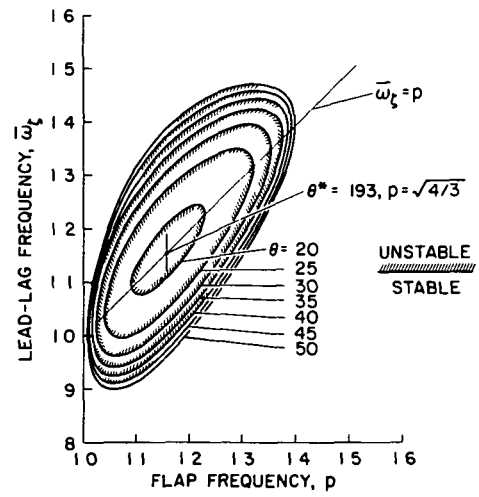

Figure 4. - Stability boundaries for basic flap-lag equations, R = 0.0.

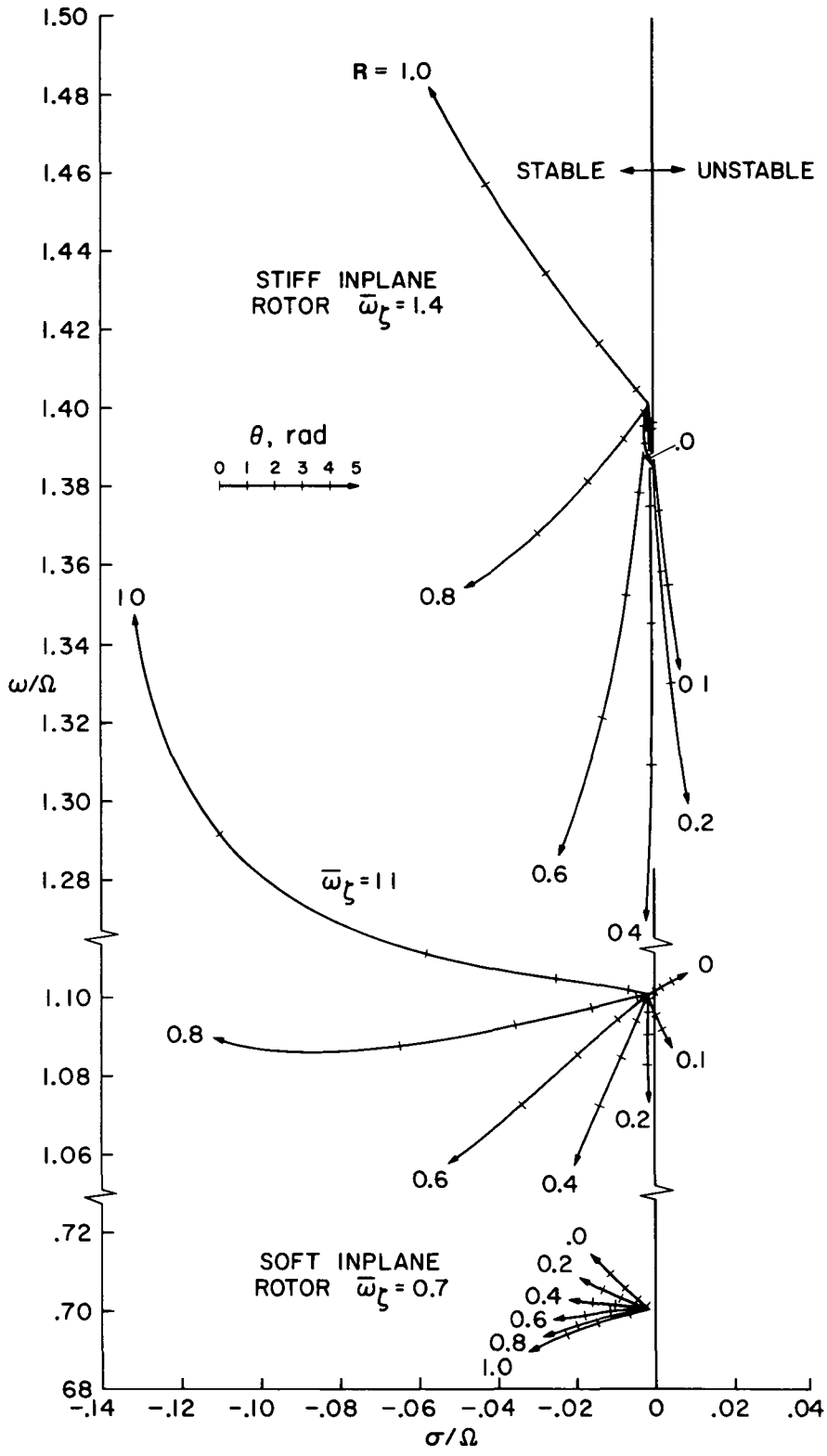

Figure 5. - Locus of lead-lag mode roots with increasing pitch angle for flap-lag equations with variable elastic coupling, R ≠ 0.0, p = $\sqrt{4/3}$.

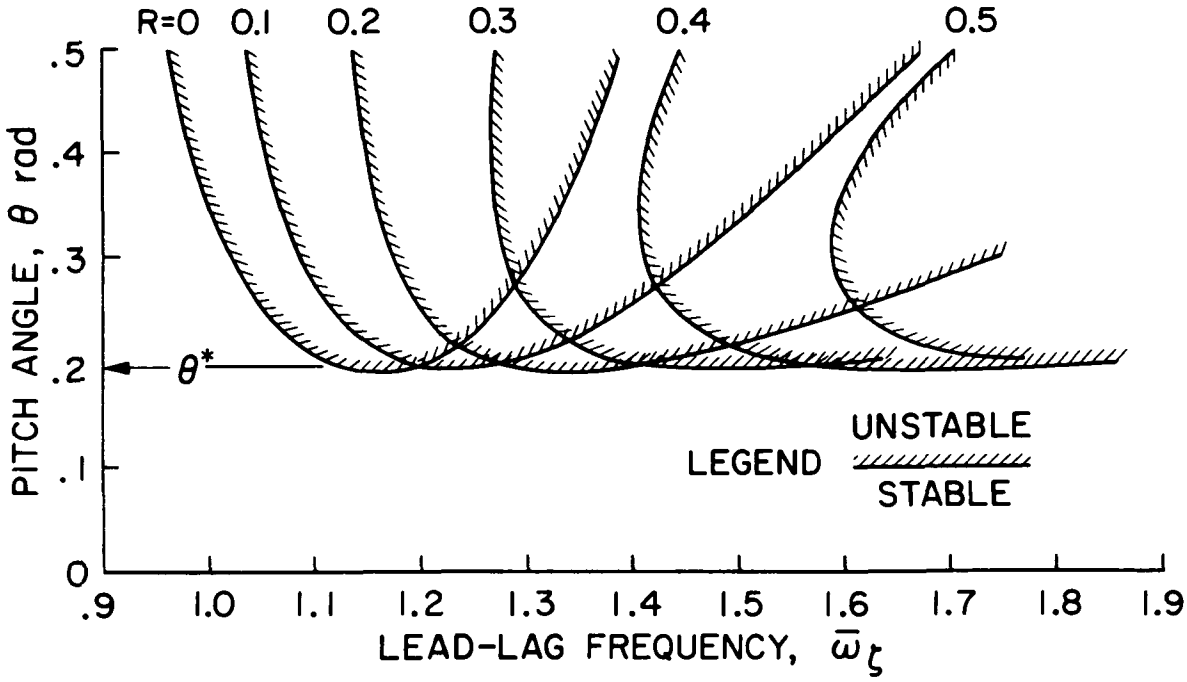

Figure 6. - Stability boundaries for flap-lag equations with variable elastic coupling, R ≠ 0.0, p = $\sqrt{4/3}$.

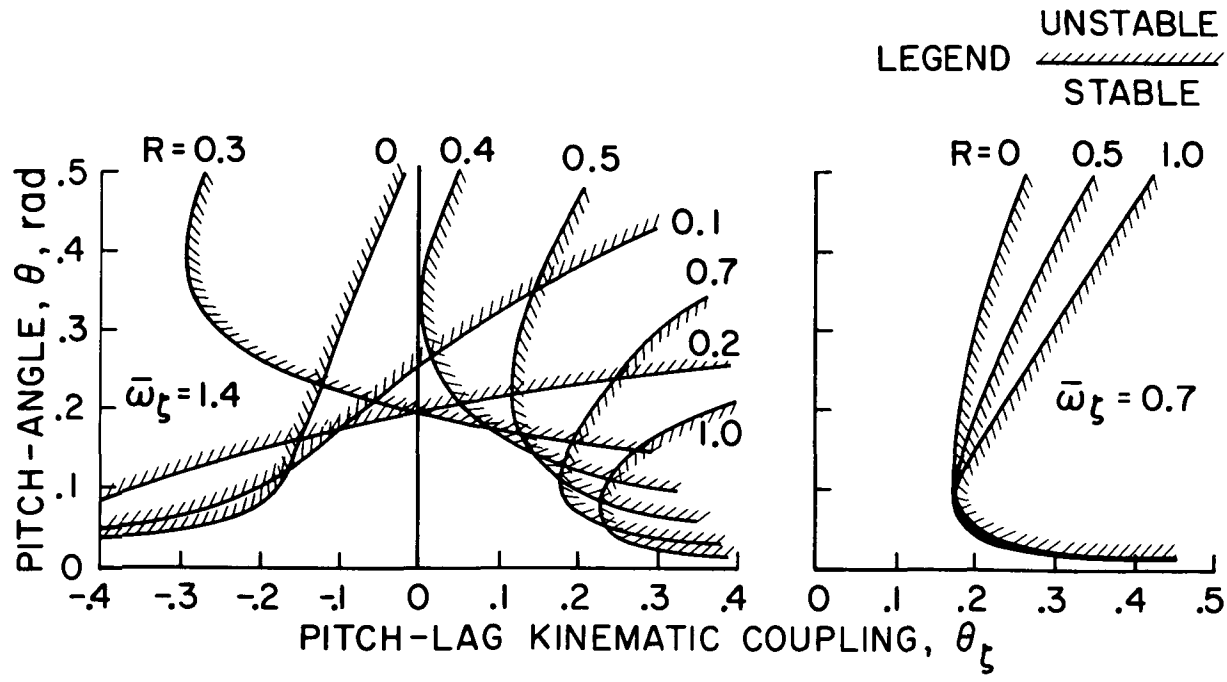

Figure 7. - Stability boundaries for flap-lag equations with variable elastic coupling and kinematic pitch-lag coupling, p = $\sqrt{4/3}$.

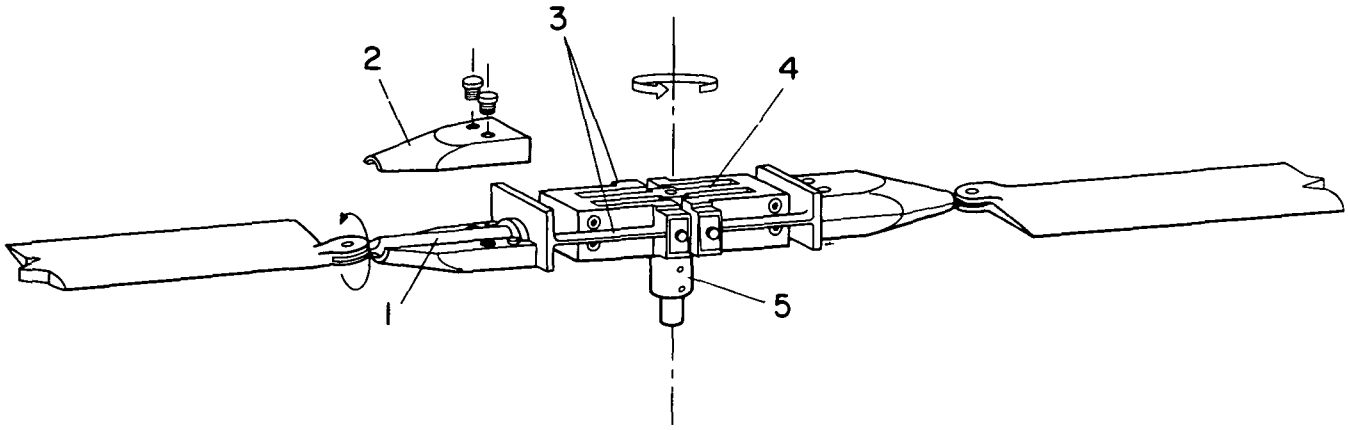

1 - PITCH CHANGE (ROTATION OF BLADE ROOT WITHIN CLAMP)
2 - ROOT CLAMP
3 - FLAP FLEXURES, TWO EACH BLADE (℄ AT .047R)
4 - LEAD LAG FLEXURES (℄ AT .038R)
5 - HUB

Figure 8. - Experimental rotor hub.

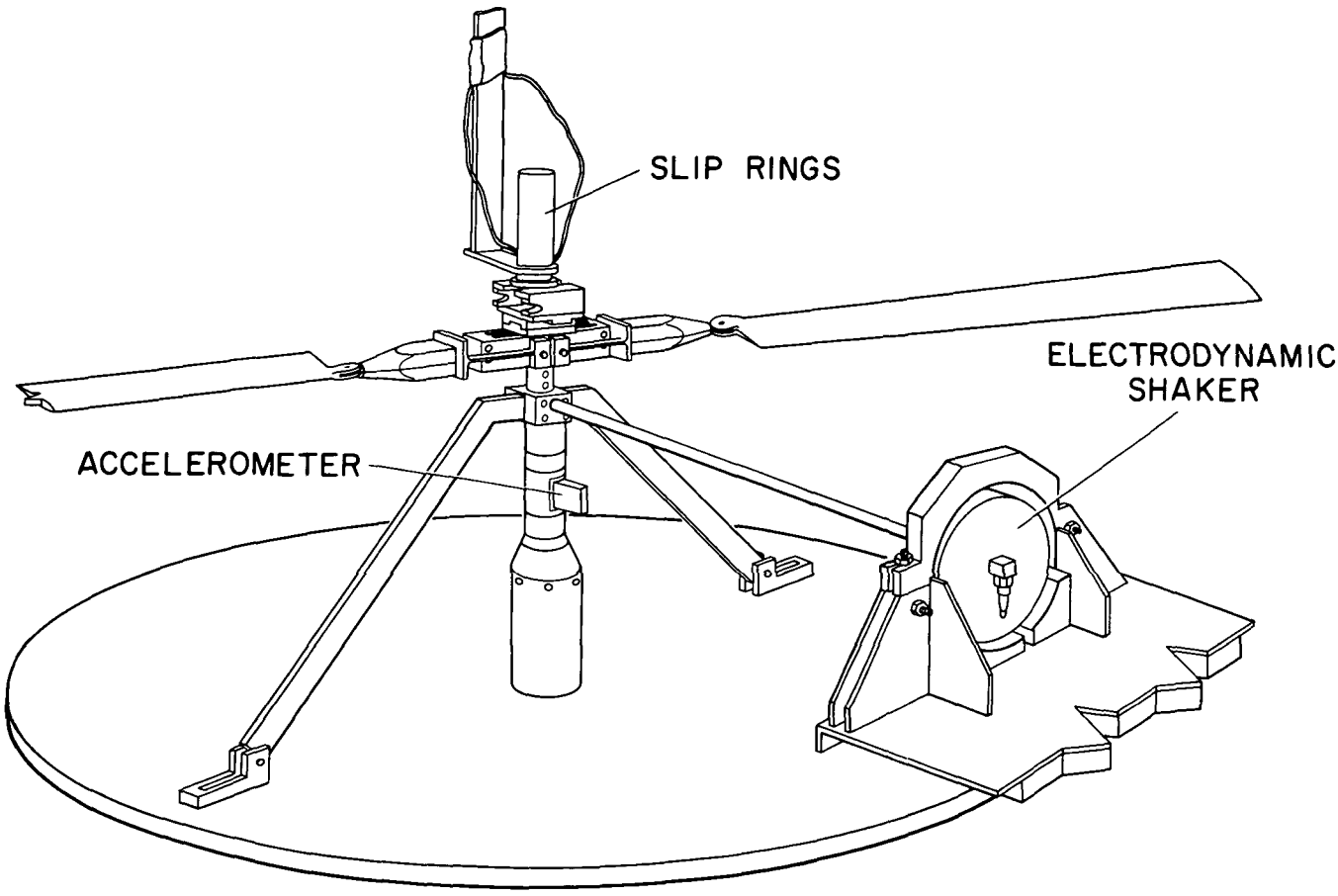

Figure 9. - Experimental rotor test set-up.

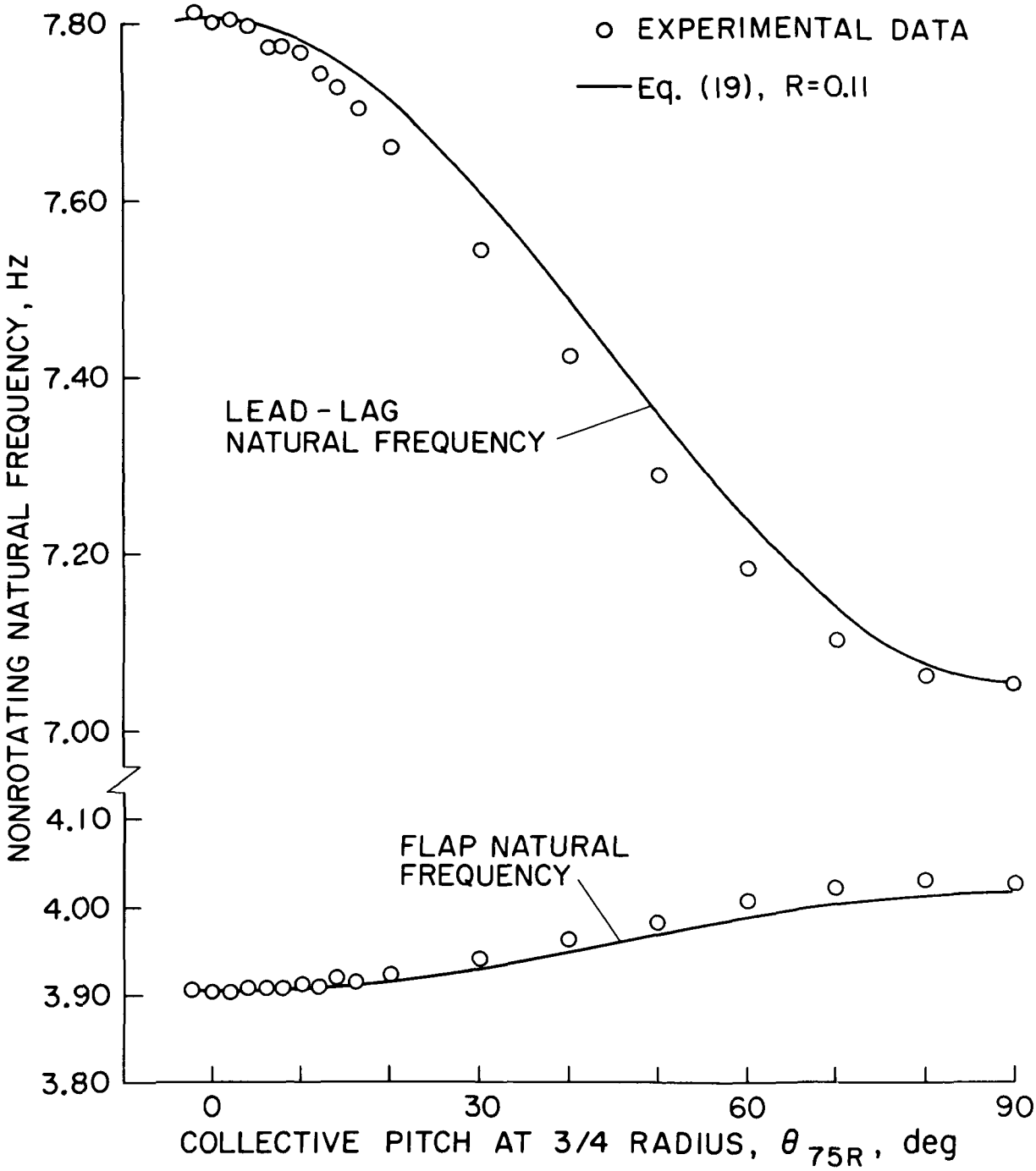

Figure 10. - Nonrotating flap and lead-lag natural frequency variation with collective pitch angle.

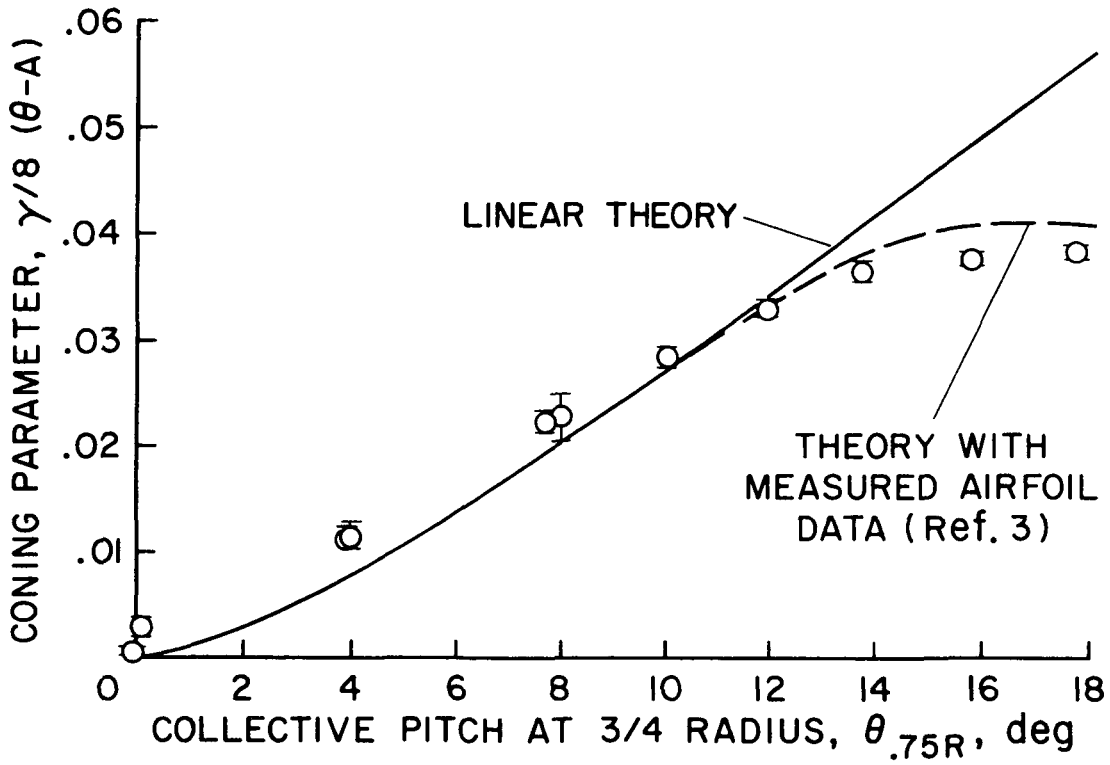

Figure 11. - Steady blade coning angle variation with collective pitch angle.

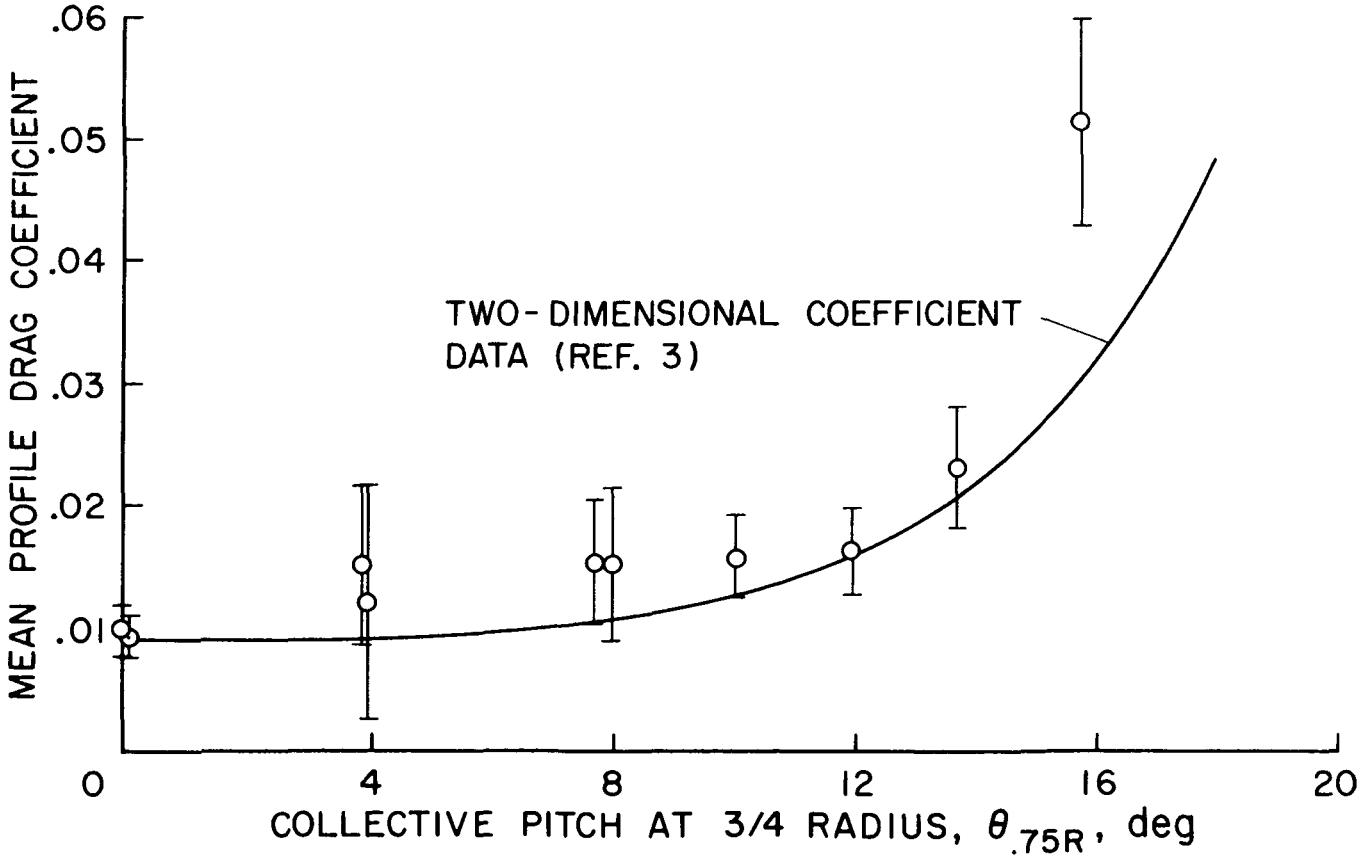

Figure 12. - Mean profile drag coefficient variation with collective pitch angle.

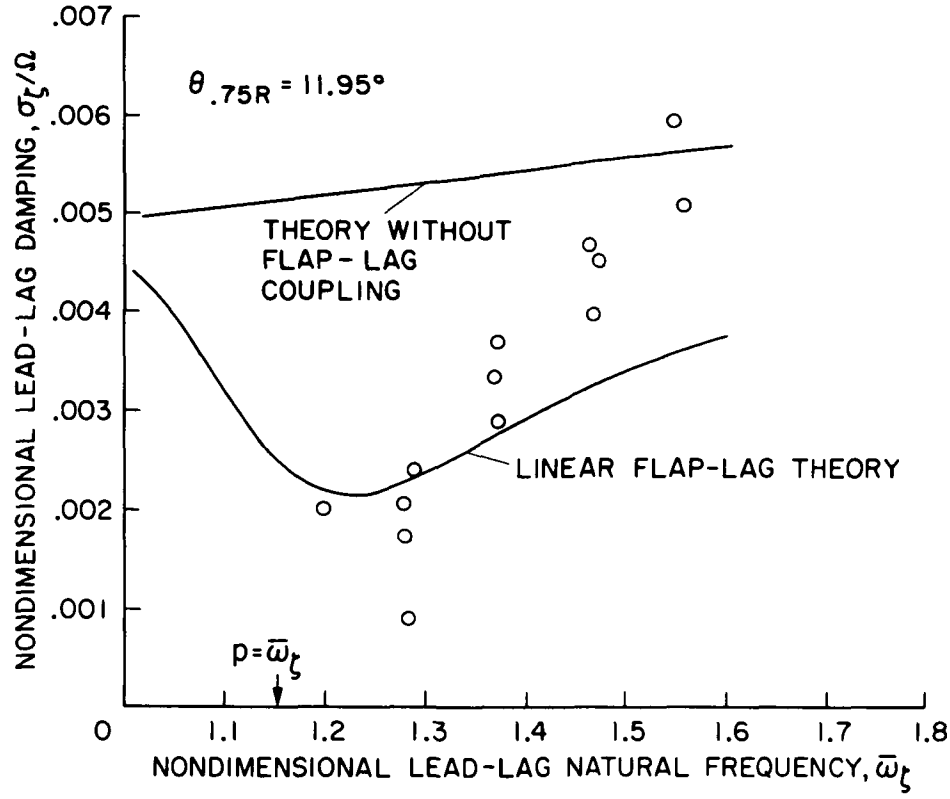

Figure 13. - Nondimensional lead-lag damping variation with blade nondimensional lead-lag natural frequency.

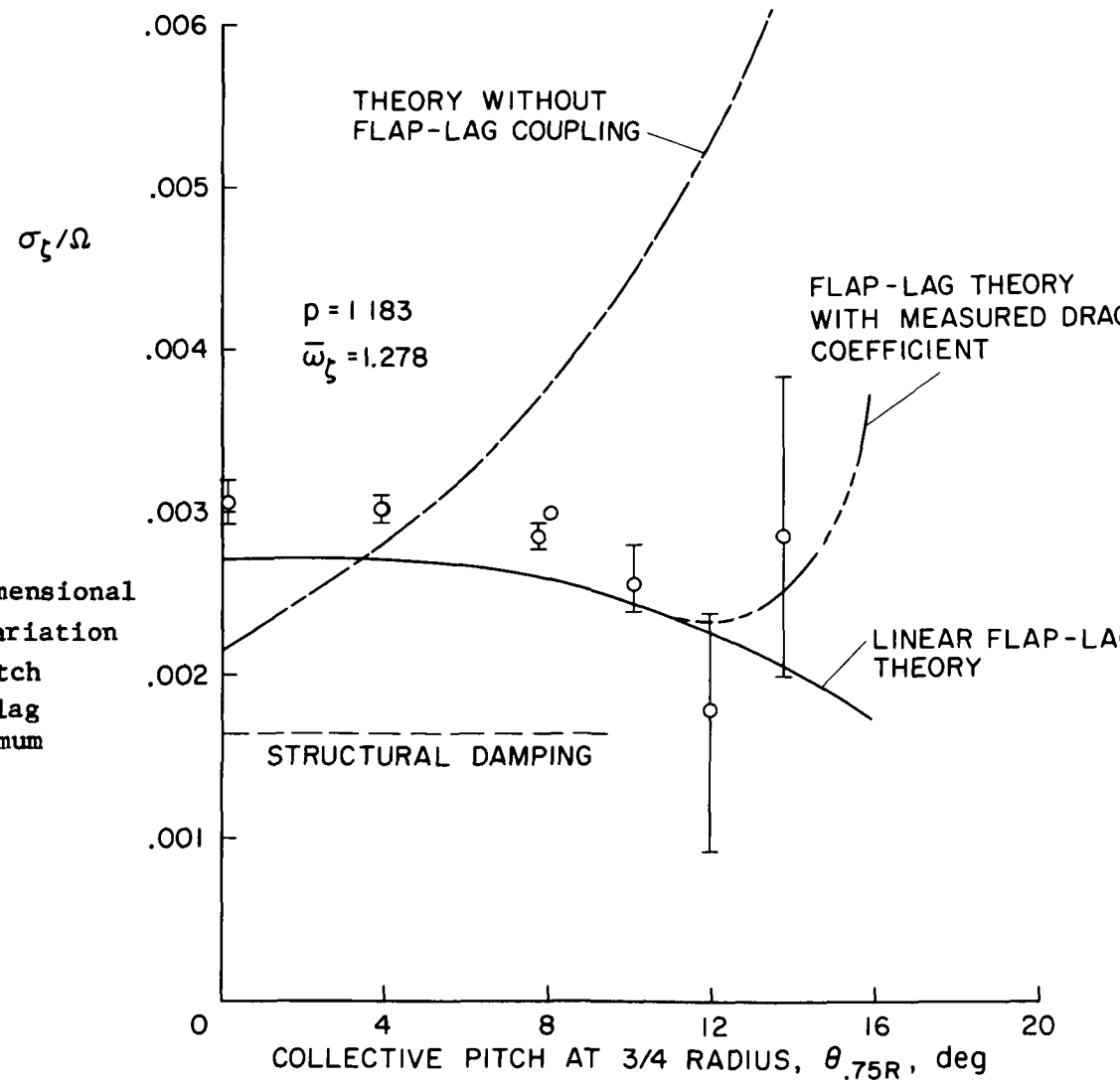

Figure 14. - Nondimensional lead-lag damping variation with collective pitch angle at the lead-lag frequency for minimum damping.